Search for relativistic magnetic monopoles with five years of the ANTARES detector data

A. Albert[a], M. André[b], M. Anghinolfi[c], G. Anton[d], M. Ardid[e], J.-J. Aubert[f], T. Avgitas[g], B. Baret[g], J. Barrios-Martí[h], S. Basa[i], V. Bertin[f], S. Biagi[j], R. Bormuth[k,l], S. Bourret[g], M.C. Bouwhuis[k], R. Bruijn[k,m], J. Brunner[f], J. Busto[f], A. Capone[n,o], L. Caramete[p], J. Carr[f], S. Celli[n,o,q], T. Chiarusi[r], M. Circella[s], J.A.B. Coelho[g], A. Coleiro[g,h], R. Coniglione[j], H. Costantini[f], P. Coyle[f], A. Creusot[g], A. Deschamps[t], G. De Bonis[n,o], C. Distefano[j], I. Di Palma[n,o], A. Domi[c,u], C. Donzaud[g,v], D. Dornic[f], D. Drouhin[a], T. Eberl[d], I. El Bojaddaini[w], D. Elsässer[x], A. Enzenhöfer[f], I. Felis[e], L.A. Fusco[r,y], S. Galatà[g], P. Gay[z,g], V. Giordano[aa], H. Glotin[ab,ac], T. Grégoire[g], R. Gracia Ruiz[g], K. Graf[d], S. Hallmann[d], H. van Haren[ad], A.J. Heijboer[k], Y. Hello[t], J.J. Hernández-Rey[h], J. Hößl[d], J. Hofestädt[d], C. Hugon[c,u], G. Illuminati[h], C.W James[d], M. de Jong[k,l], M. Jongen[k], M. Kadler[x], O. Kalekin[d], U. Katz[d], D. Kießling[d], A. Kouchner[g,ac], M. Kreter[x], I. Kreykenbohm[ae], V. Kulikovskiy[f,af], C. Lachaud[g], R. Lahmann[d], D. Lefèvre[ag], E. Leonora[aa,ah], M. Lotze[h], S. Loucatos[ai,g], M. Marcelin[i], A. Margiotta[r,y], A. Marinelli[aj,ak], J.A. Martínez-Mora[e], R. Mele[al,am], K. Melis[k,m], T. Michael[k], P. Migliozzi[al], A. Moussa[w], S. Navas[ap], E. Nezri[i], M. Organokov[an], G.E. Păvălaş[p], C. Pellegrino[r,y], C. Perrina[n,o], P. Piattelli[j], V. Popa[p], T. Pradier[an], L. Quinn[f], C. Racca[a], G. Riccobene[j], A. Sánchez-Losa[s], M. Saldaña[e], I. Salvadori[f], D. F. E. Samtleben[k,l], M. Sanguineti[c,u], P. Sapienza[j], F. Schüssler[ai], C. Sieger[d], M. Spurio[r,y], Th. Stolarczyk[ai], M. Taiuti[c,u], Y. Tayalati[ao], A. Trovato[j], D. Turpin[f], C. Tönnis[h], B. Vallage[ai,g], V. Van Elewyck[g,ac], F. Versari[r,y], D. Vivolo[al,am], A. Vizzoca[n,o], J. Wilms[ae], J.D. Zornoza[h], and J. Zúñiga[h]

[a]GRPHE - Université de Haute Alsace - Institut universitaire de technologie de Colmar, 34 rue du Grillenbreit BP 50568 - 68008 Colmar, France
[b]Technical University of Catalonia, Laboratory of Applied Bioacoustics, Rambla Exposició, 08800 Vilanova i la Geltrú, Barcelona, Spain
[c]INFN - Sezione di Genova, Via Dodecaneso 33, 16146 Genova, Italy

[d]Friedrich-Alexander-Universität Erlangen-Nürnberg, Erlangen Centre for Astroparticle Physics, Erwin-Rommel-Str. 1, 91058 Erlangen, Germany
[e]Institut d'Investigació per a la Gestió Integrada de les Zones Costaneres (IGIC) - Universitat Politècnica de València. C/ Paranimf 1, 46730 Gandia, Spain
[f]Aix Marseille Univ, CNRS/IN2P3, CPPM, Marseille, France
[g]APC, Univ Paris Diderot, CNRS/IN2P3, CEA/Irfu, Obs de Paris, Sorbonne Paris Cité, France
[h]IFIC - Instituto de Física Corpuscular (CSIC - Universitat de València) c/ Catedrático José Beltrán, 2 E-46980 Paterna, Valencia, Spain
[i]LAM - Laboratoire d'Astrophysique de Marseille, Pôle de l'Étoile Site de Château-Gombert, rue Frédéric Joliot-Curie 38, 13388 Marseille Cedex 13, France
[j]INFN - Laboratori Nazionali del Sud (LNS), Via S. Sofia 62, 95123 Catania, Italy
[k]Nikhef, Science Park, Amsterdam, The Netherlands
[l]Huygens-Kamerlingh Onnes Laboratorium, Universiteit Leiden, The Netherlands
[m]Universiteit van Amsterdam, Instituut voor Hoge-Energie Fysica, Science Park 105, 1098 XG Amsterdam, The Netherlands
[n]INFN - Sezione di Roma, P.le Aldo Moro 2, 00185 Roma, Italy
[o]Dipartimento di Fisica dell'Università La Sapienza, P.le Aldo Moro 2, 00185 Roma, Italy
[p]Institute for Space Science, RO-077125 Bucharest, Măgurele, Romania
[q]Gran Sasso Science Institute, Viale Francesco Crispi 7, 00167 L'Aquila, Italy
[r]INFN - Sezione di Bologna, Viale Berti-Pichat 6/2, 40127 Bologna, Italy
[s]INFN - Sezione di Bari, Via E. Orabona 4, 70126 Bari, Italy
[t]Géoazur, UCA, CNRS, IRD, Observatoire de la Côte d'Azur, Sophia Antipolis, France
[u]Dipartimento di Fisica dell'Università, Via Dodecaneso 33, 16146 Genova, Italy
[v]Université Paris-Sud, 91405 Orsay Cedex, France
[w]University Mohammed I, Laboratory of Physics of Matter and Radiations, B.P.717, Oujda 6000, Morocco
[x]Institut für Theoretische Physik und Astrophysik, Universität Würzburg, Emil-Fischer Str. 31, 97074 Würzburg, Germany
[y]Dipartimento di Fisica e Astronomia dell'Università, Viale Berti Pichat 6/2, 40127 Bologna, Italy
[z]Laboratoire de Physique Corpusculaire, Clermont Université, Université Blaise Pascal, CNRS/IN2P3, BP 10448, F-63000 Clermont-Ferrand, France
[aa]INFN - Sezione di Catania, Viale Andrea Doria 6, 95125 Catania, Italy
[ab]LSIS, Aix Marseille Université CNRS ENSAM LSIS UMR 7296 13397 Marseille, France; Université de Toulon CNRS LSIS UMR 7296, 83957 La Garde, France
[ac]Institut Universitaire de France, 75005 Paris, France
[ad]Royal Netherlands Institute for Sea Research (NIOZ), Landsdiep 4, 1797 SZ 't Horntje (Texel), The Netherlands
[ae]Dr. Remeis-Sternwarte and ECAP, Universität Erlangen-Nürnberg, Sternwartstr. 7, 96049 Bamberg, Germany
[af]Moscow State University, Skobeltsyn Institute of Nuclear Physics, Leninskie gory, 119991 Moscow, Russia
[ag]Mediterranean Institute of Oceanography (MIO), Aix-Marseille University, 13288, Marseille, Cedex 9, France; Université du Sud Toulon-Var, CNRS-INSU/IRD UM 110, 83957, La Garde Cedex, France
[ah]Dipartimento di Fisica ed Astronomia dell'Università, Viale Andrea Doria 6, 95125 Catania, Italy
[ai]Direction des Sciences de la Matière - Institut de recherche sur les lois fondamentales de l'Univers - Service de Physique des Particules, CEA Saclay, 91191 Gif-sur-Yvette Cedex, France
[aj]INFN - Sezione di Pisa, Largo B. Pontecorvo 3, 56127 Pisa, Italy
[ak]Dipartimento di Fisica dell'Università, Largo B. Pontecorvo 3, 56127 Pisa, Italy
[al]INFN - Sezione di Napoli, Via Cintia 80126 Napoli, Italy
[am]Dipartimento di Fisica dell'Università Federico II di Napoli, Via Cintia 80126, Napoli, Italy
[an]Université de Strasbourg, CNRS, IPHC UMR 7178, F-67000 Strasbourg, France
[ao]University Mohammed V in Rabat, Faculty of Sciences, 4 av. Ibn Battouta, B.P. 1014, R.P. 10000 Rabat, Morocco

[ap]Departamento de Física Teórica y del Cosmos & C.A.F.P.E., Universidad de Granada. Av. Severo Ochoa s/n, 18071 Granada, Spain

March 2, 2017

Abstract

A search for magnetic monopoles using five years of data recorded with the ANTARES neutrino telescope from January 2008 to December 2012 with a total live time of 1121 days is presented. The analysis is carried out in the range $\beta > 0.6$ of magnetic monopole velocities using a strategy based on run-by-run Monte Carlo simulations. No signal above the background expectation from atmospheric muons and atmospheric neutrinos is observed, and upper limits are set on the magnetic monopole flux ranging from 5.7×10^{-16} to 1.5×10^{-18} cm$^{-2}\cdot$ s$^{-1}\cdot$ sr^{-1}.

Keywords : Magnetic monopole, Neutrino telescope, ANTARES

1 Introduction

Magnetic monopoles could play an important role in contexts such as cosmology and particle physics. Particles carrying only one magnetic pole were hypothesized by P. A. M. Dirac in 1931 [1], who established a relation between the electric (e) and the magnetic (g) elementary charges:

$$g = k \cdot g_D = k \cdot \frac{e}{2 \cdot \alpha}, \tag{1}$$

where g_D is the Dirac charge, k is an integer, and α is the fine structure constant. Dirac demonstrated that the existence of a magnetic monopole could explain the quantization of the electric charge. Just as electric charges can be positive or negative, magnetism comes with two poles, North and South. Theory suggests that magnetism could be a property of elementary particles. However, the negative and positive electric charges can be isolated, while an isolated magnetic charge has not been observed so far. In 1974, G. 't Hooft [2] and A. M. Polyakov [3] showed that the electric charge is naturally quantized in Grand Unification Theories. Magnetic monopoles appear at the phase transition corresponding to the spontaneous breaking of the unified group into subgroups, one of which is U(1), describing electromagnetism. Additionally, magnetic monopoles which belong to the family of topological defects might contribute to cosmological models in the context of inflation [4].

Different experiments worldwide have been trying to hunt these particles, with no positive evidence so far [5]. However, analogs of magnetic monopoles may be observable in quantum fluids. M. W. Ray et al. [6] performed an experiment in which they manipulated a gas of rubidium atoms prepared in a non-magnetic state close to absolute zero temperature. Under these extreme conditions, they were able to create a system behaving as a magnetic monopole in the quantum-mechanical field that describes the gas. This experiment established important characteristics of magnetic monopoles, supporting the possibility of their existence. Other experiments searched for magnetic monopoles in lunar material and polar volcanic rocks, and established upper limits on their density and cross section [7, 8].

Recently it was realized that electroweak interactions allow magnetic monopole solutions, also with multiple elementary magnetic charges [5]. The mass of these magnetic monopoles has been estimated to be less than 10 TeV, making it a very good candidate for searches at the CERN Large Hadron Collider (LHC). The ATLAS collaboration [9] searched for magnetic monopoles as highly ionizing particles produced in proton-proton collisions, leading to new cross section upper limits for spin 1/2 and spin 0 particles. MoEDAL is a dedicated experiment searching for magnetic monopoles produced in high-energy collisions at the LHC using stacks of nuclear-track detectors and a trapping detector. Recently, limits on magnetic monopoles production cross sections have been reported both for the 8 TeV and 13 TeV LHC runs [10, 11].

Magnetic monopoles of a certain mass range, thanks to their magnetic charge, could be accelerated to relativistic speeds. Thus, several searches were carried out with neutrino telescopes without any positive result leading to upper limits on the magnetic monopole flux below the theoretical Parker bound [12]. The IceCube collaboration has set upper limits on the flux for relativistic magnetic monopoles ranging from 1.55×10^{-18} to 10.39×10^{-18} $\mathrm{cm}^{-2} \cdot \mathrm{s}^{-1} \cdot \mathrm{sr}^{-1}$ [13]. The ANTARES neutrino telescope [14] was completed in 2008 and the collected data can be used to search for magnetic monopoles with energies high enough to yield Cherenkov light emission. The results of the analysis published in [15] using a data set of 116 days live time, lead to upper limits on the monopole flux in the range between 1.3×10^{-17} and 5.7×10^{-16} $\mathrm{cm}^{-2} \cdot \mathrm{s}^{-1} \cdot \mathrm{sr}^{-1}$ for magnetic monopoles with $\beta = v/c > 0.6$, where v is the magnetic monopole speed and c is the speed of light in vacuum.

In this paper, a new analysis is presented, based on an enlarged data set of 1121 days collected from 2008 to 2012, increasing by a factor of $\sim$10 the live time of the previous published result. This analysis is based on a

new selection of cuts, yielding a better separation of the magnetic monopole signal from the background of atmospheric muons and neutrinos. Further, it relies on a new simulation strategy that reproduces each data run individually, allowing for an accurate reproduction of the data taking conditions.

The paper is organized as follows: a brief description of the ANTARES telescope and the expected signatures of magnetic monopoles are given in sections 2 and 3, respectively. The simulation and reconstruction algorithms are described in sections 4 and 5. The magnetic monopole-sensitive observables, the selection strategy and the upper limit calculation are discussed in sections 6 and 7. Finally, the results are presented and discussed in section 8.

2 The ANTARES telescope

The ANTARES detector [14] is an undersea neutrino telescope anchored 2475 m below the surface of the Mediterranean Sea and 40 km offshore from Toulon (France). It consists of 12 detection lines with 25 storeys per line and 3 optical modules (OMs) with 10-inch photomultipliers (PMTs) per storey. The detection lines are 450 m long and spaced 60−75 m apart horizontally. The main channel for neutrino detection is via the muons produced from high-energy muon neutrinos interacting inside, or in the vicinity of the detector. These muons move at relativistic velocities and induce the emission of Cherenkov light along their paths, detected by the optical modules. PMT signals corresponding to a charge above a threshold of 0.3 photo-electrons are integrated with a time window of 40 ns, digitised and denoted as hits. The readout of OMs is performed in the storey's Local Control Module, which collects the data in packages of 104 ms. These packages are sent to an on-chore farm of computers for further data processing and filtering. Each detector storey has one local clock that is synchronized to the on-shore master clock [16]. Furthermore, at the computer farm a system of triggers is applied on the data (see section 5), selecting signatures which may correspond to the passage of reletivistic particles.

3 Detection of magnetic monopoles

The signature of a magnetic monopole in a neutrino telescope like ANTARES is similar to that of a highly energetic muon. Thus, as in the case of electrically-charged particles, magnetically-charged particles induce the polarization of the dielectric medium. Coherent light emission (Cherenkov

effect) is induced by the restoring medium if the particle travels with a speed above the Cherenkov threshold $\beta_{th} = 1/n$, where n is the refractive index of the medium [17]. In water the threshold is $\beta_{th} \approx 0.74$. The number of photons emitted from a magnetic monopole with magnetic charge g in a small interval of path length, dx, and in the range $d\lambda$ of wavelength, for $\beta \geq \beta_{th}$ can be expressed as

$$\frac{d^2 n_\gamma}{d\lambda dx} = \frac{2\pi\alpha}{\lambda^2} \left(\frac{ng}{e}\right)^2 \left(1 - \frac{1}{n^2\beta^2}\right), \tag{2}$$

where n_γ is the number of photons emitted and λ is their wavelength; the remaining quantities are already defined in Eq. (1). For a given velocity, the Cherenkov radiation yield by a magnetic monopole is a factor $\left(\frac{ng}{Ze}\right)^2$ larger than that from a particle with electric charge Ze. In addition to a different intensity of Cherenkov radiation, the radiation is polarized differently for a magnetic monopole than for an electric charge. Thus, for the refractive index of sea water, fast monopoles with $g = g_D$ are expected to emit about 8550 times more Cherenkov photons than relativistic muons.

In addition to the direct Cherenkov radiation, magnetic monopoles can knock off atomic electrons (δ-ray electrons) that can have velocities above the Cherenkov threshold, contributing to the total light yield. For the production of δ-electrons, the differential cross-section of Kasama, Yang and Goldhaber (KYG) [18] or the more conservative (in terms of photon yield) Mott cross section [19] can be used. In this work, the Mott cross section is used, starting for the minimum velocity of $\beta = 0.5945$. The contributions to the light yield from these mechanisms are shown in Fig. 1. Contributions from radioluminescence of water, pair production, Bremsstrahlung and photo-nuclear reactions induced by relativistic magnetic monopoles are negligible compared to the direct and indirect Cherenkov light presented in Fig. 1, and are not taken into account in this analysis.

In neutrino telescopes, the solid angle region corresponding to down-going events is dominated by the background of atmospheric muons. In particular, muons in bundle can easily be misidentified with the passage of a relativistic highly ionizing particle. On the opposite, the solid angle region corresponding to up-going events is almost background free, apart from the events induced by atmospheric neutrinos and the surviving down-going atmospheric muons misreconstructed as up-going. Due to the energy spectrum of atmospheric muon neutrinos, they usually induce minimum ionizing muons that can be easily distinguished from fast magnetic monopoles. In order to suppress the irreducible background of atmospheric muons, only up-going magnetic monopoles were considered.

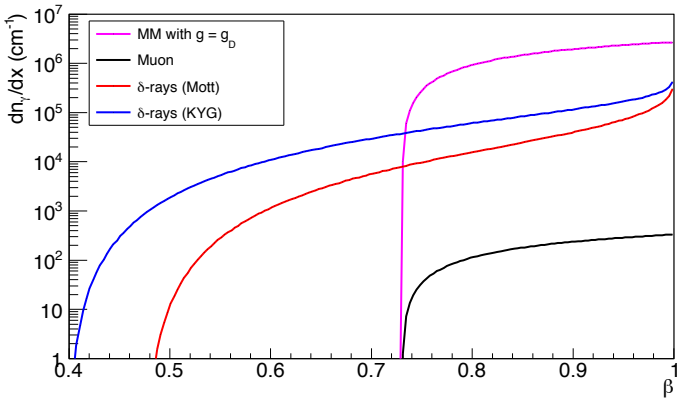

Figure 1: The total number of Cherenkov photons with wavelengths between 300 and 600 nm that are directly produced per centimeter path length by a magnetic monopole (MM) with $g = g_D$, as a function of the monopole velocity (β). The number of photons produced by δ-rays with Mott cross section model [19] and KYG cross section model [18] and by a minimum ionizing muon are also shown.

S. P. Ahlen [20] has established the magnetic monopole equivalent of the Bethe-Bloch formula that describes the energy loss in the passage of a heavy electric charge by ionization and excitation in a non-conductive medium. Thus, the energy loss of a magnetic monopole crossing the Earth could be estimated using the simplified density profile established by Derkaoui et al. [21]. Despite the high energy loss when crossing the Earth, magnetic monopoles would remain relativistic and detectable as up-going events if their mass exceeds 10^{10} GeV/c^2 (see for instance Fig. 3 of [5]), because of the large kinetic energy attained as they are accelerated by Galactic magnetic fields up to 1.7×10^{13} GeV [22] for a minimum magnetic charge. Due to this fact, only magnetic monopoles with a mass $M \leq 10^{14}$ GeV/c^2 can be detected in neutrino telescopes. Thus, the limits presented in this paper hold for magnetic monopole masses in the range 10^{10} GeV/$c^2 < M \leq 10^{14}$ GeV/c^2.

4 Monte Carlo simulation

In this section, the simulation of the magnetic monopole signal and the atmospheric (neutrino and muon) background events are discussed.

4.1 Magnetic monopole simulation

Up-going magnetic monopoles with one unit of Dirac charge, $g = g_D$, have been simulated using nine equal width ranges of velocity in the region $\beta = [0.5945, 0.9950]$. The nine intervals of the velocity are defined in the first column of Table 1.

Magnetic monopoles have been simulated using a Monte Carlo program based on GEANT3 [23]. The simulation is independent of the magnetic monopole mass and the incoming direction of magnetic monopoles was distributed isotropically over the lower hemisphere. The propagation and detection of emitted photons is processed inside a *can*, i.e a virtual cylindrical surface surrounding the instrumented volume around the detector. A radius of 480 m is chosen to take into account the large amount of light emitted by a magnetic monopole.

4.2 Background simulation

The main source of background comes from up-going muons induced by atmospheric neutrinos and down-going atmospheric muons wrongly reconstructed as up-going tracks. The simulation of atmospheric muons is carried out using the generator MUPAGE [24] based on the parametrisation of the angle and energy distributions of muons under-water as a function of the muon bundle multiplicity [25]. MUPAGE produces muon events on the surface of the can.

Up-going atmospheric neutrinos from the decay of pions and kaons are simulated using the package GENHEN [26, 27] assuming the model from the Bartol group [28, 29] which does not include the decay of charmed particles.

The analysis presented in this paper is based on a run-by-run Monte Carlo simulation [30], which takes into consideration the real data taking conditions of the detector (e.g. sea water conditions, bioluminescence variability, detector status).

5 Trigger and reconstruction

The applied triggers are based on local coincidences defined as the occurrence of either two hits on two separate optical modules of a single storey within 20 ns, or one single hit of large amplitude, typically more than 3 photo-electrons. The trigger used for this analysis is defined as a combination of two local coincidences in adjacent or next-to-adjacent storeys within 100 ns or 200 ns, respectively. In this analysis, only events passing such a

trigger, well suited for magnetic monopoles, are considered.

The event reconstruction has been done with a slightly modified version of the algorithm described in [31]. By default it assumes that particles travel at the speed of light. In order to improve the sensitivity for magnetic monopoles travelling with lower velocities, the algorithm was modified such as to leave the reconstructed velocity of the particle β_{fit} as a free parameter to be derived by the track fit.
The algorithm performs two independent fits: a track fit and a bright-point fit. The former reconstructs particles crossing the detector, while the latter reconstructs showering events, as those induced by ν_e charged current interactions. Both fits minimize the same χ^2 quality function, thus, two parameters defining the quality of these reconstructions are introduced, $t\chi^2$ for the track fit, and $b\chi^2$ for the bright-point fit.

Some basic quality cuts have been applied to the data to ensure good data taking conditions [32]. To avoid any experimental bias, the search strategy is based on a blind analysis. The selection cuts applied on the analysis are established on Monte Carlo simulations and using a test data sample of about 10% of the total data set, equivalent to 109 days out of the total 1121 days of live time. These runs are not used later for setting the limits.

In the following comparisons between the test data sample and simulation, the full collection of Monte Carlo runs is used, and the 10% of test data is scaled to the total live time. Fig. 2 shows the distribution of the reconstructed velocity β_{fit} for magnetic monopole events, atmospheric muons and neutrinos and compared to the test data sample. The neutrino distribution represents electron neutrinos and muon neutrinos for both neutral and charged currents.

6 Event selection

In order to remove the bulk of down-going events, only up-going events with reconstructed zenith angles $\leq 90^\circ$ are selected (Fig. 3). Thus, the comparison shows a good agreement between the test data sample and simulation. Additional cuts on the track fit quality parameter are implemented to remove misreconstructed atmospheric muon tracks. In particular, the requirement $t\chi^2 \leq b\chi^2$ is applied to favour events reconstructed as a track rather than those reconstructed as a bright point.
The further event selections were optimized for different monopole velocities. A different event selection was performed for each of the nine bins of

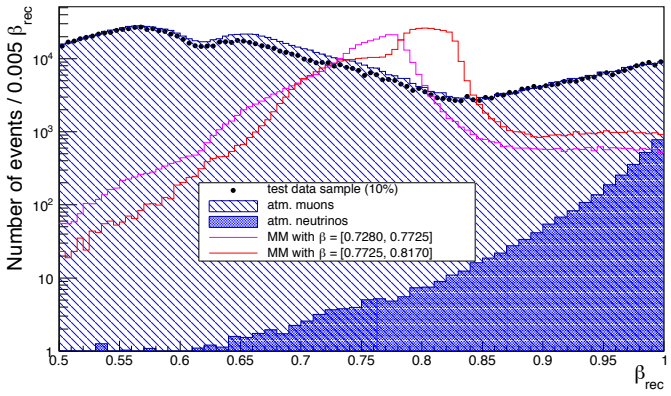

Figure 2: The distribution of the reconstructed β_{fit} for atmospheric muons, atmospheric neutrinos (hatched and full histograms, respectively) and data (points with error bars). For comparison, the distributions of the reconstructed β_{fit} for magnetic monopoles simulated in the velocity ranges $[0.7280, 0.7725]$ (magenta histogram) and $[0.7725, 0.8170]$ (red histogram) are also shown. All distributions correspond to events reconstructed as upgoing.

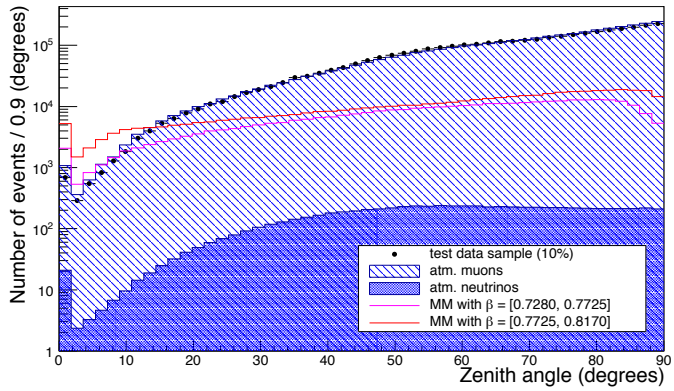

Figure 3: Reconstructed zenith angle for atmospheric muons, atmospheric neutrinos (hatched and full histograms, respectively) and data (points with error bars). For comparison, the distributions of the reconstructed zenith angle for magnetic monopoles simulated in the velocity ranges $[0.7280, 0.7725]$ (magenta histogram) and $[0.7725, 0.8170]$ (red histograms) are also shown. The peak at zenith $= 0$ represents wrongly reconstructed events.

β reported in the first column of Table 1.

The modified reconstruction algorithm which treats β_{fit} as a free parameter was used only in the regions of low velocities between $\beta = 0.5945$ and $\beta = 0.8170$ (five bins). Thus, magnetic monopoles with these velocities could be distinguished from particles traveling with the speed of light ($\beta_{fit} = 1$). For each of the five low beta bins, only events reconstructed with β_{fit} in the range of simulated β were used in the final selection. For example, at the range $\beta = [0.5945, 0.6390]$, only events with reconstructed velocity $\beta_{fit} = [0.5945, 0.6390]$ were selected.

In the high velocity interval ranging from $\beta = 0.8170$ to $\beta = 0.9950$ (four bins), the β_{fit} is not a discriminant variable anymore. However, magnetic monopoles emit a large amount of light compared to that emitted from other particles, which allows them to be distinguished.

In the used reconstruction algorithm, the hits from the optical modules belonging to the same storey are summed together to form a *track hit*. The coordinates of its position are coincident with the center of the storey, the time is equal to the time of the first hit and the charge equal to the sum of the hits charges. For all velocity bins, the number of storeys with selected track hits N_{hit}, is used as a powerful discriminant variable since it refers to the amount of light emitted in the event (see Fig. 4).

A second discriminative variable is introduced to further reduce the background, in particular for the velocities below the threshold for direct Cherenkov radiation where the light emission is lower. This variable, named α, is defined from a combination of the track fit quality parameter $t\chi^2$ and N_{hit} following [31]:

$$\alpha = \frac{t\chi^2}{1.3 + (0.04 \times (N_{hit} - N_{df}))^2}, \tag{4}$$

where N_{df} is the number of free parameters in the reconstruction algorithm. It is equal to 6 when β_{fit} is included in the reconstruction, and 5 when the velocity is not reconstructed. Example of α distribution is shown at Fig. 5. This parameter has the advantage of including the track fit quality parameter balanced with the brightness of the events, avoiding that bright events get cut by the condition applied on the $t\chi^2$ variable.

7 Optimization of cuts

The following step to suppress the atmospheric background is to use specific cuts on the N_{hit} and α parameters in order to maximize the signal-to-noise

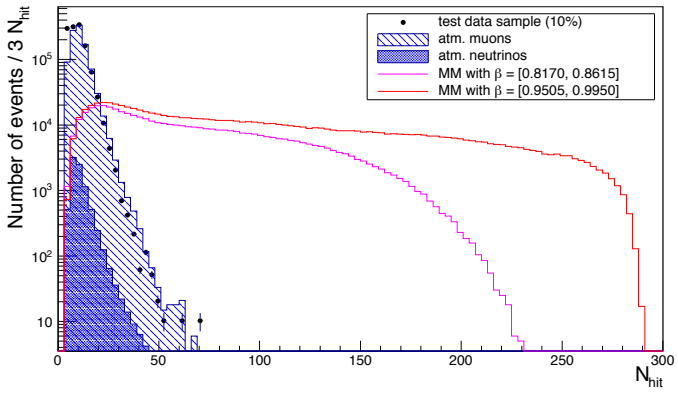

Figure 4: N_{hit} distribution for atmospheric muons, atmospheric neutrinos (hatched and full histograms, respectively) and data (points with error bars). For comparison, the distributions of N_{hit} for magnetic monopoles simulated in the velocity ranges $[0.8170, 0.8615]$ (magenta histogram) and $[0.9505, 0.9950]$ (red histogram) are also shown. At high velocities, N_{hit} provides a good descrimination for magnetic monopole signals after applying the cuts zenith $\leq 90^\circ$ and $t\chi^2 \leq b\chi^2$.

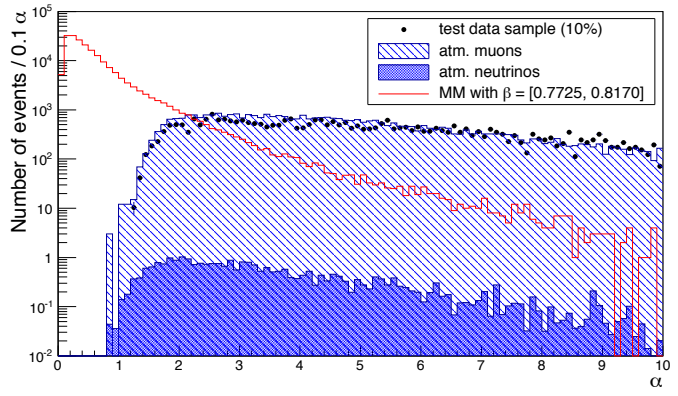

Figure 5: Distribution of the α variable for atmospheric muons, atmospheric neutrinos (hatched and full histograms, respectively) and data (points with error bars). For comparison, the distribution of the α variable for magnetic monopoles simulated in the velocity range $[0.7725, 0.8170]$ (red histogram) is also shown. Only events with reconstructed velocity $\beta_{fit} = [0.7725, 0.8170]$ were selected, and the cuts zenith $\leq 90^\circ$ and $t\chi^2 \leq b\chi^2$ have been applied.

ratio. In Fig. 6, the event distribution of α as a function of N_{hit} is shown for one range of magnetic monopole velocity. This distribution indicates that a good separation of magnetic monopole signal from background is achievable. The effect of the cuts is shown by the horizontal and vertical lines. The signal region corresponds to the left upper quadrant.

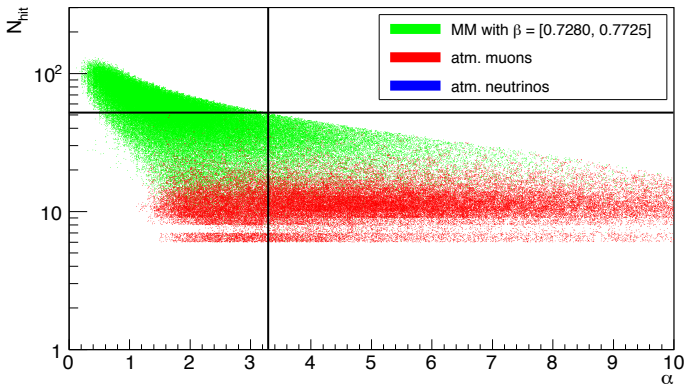

Figure 6: Two-dimensional distribution of α and N_{hit}, for atmospheric muons, atmospheric neutrinos, and magnetic monopoles simulated in the velocity range $[0.7280, 0.7725]$. The cuts zenith $\leq 90^\circ$ and $t\chi^2 \leq b\chi^2$ have been applied, as well as the cut $\beta_{fit} = [0.7280, 0.7725]$. The vertical and horizontal lines show the cuts applied after optimization. No neutrinos survived at this range of β.

The 90% confidence level interval $\mu_{90}(n_b, n_{obs})$, where n_b is the number of background events is the 90% confidence interval defined by the Feldman-Cousins approach [33]. It depends on the number of observed events n_{obs} which is not known at this point because of the blind approach. Instead, the average confidence interval $\bar{\mu}_{90}(n_b)$ is calculated, from which the sensitivity of the analysis can be derived, by assuming a Poissonian probability distribution for the number of observed events n_{obs}. The selection cuts are optimized by minimizing the so-called Model Rejection Factor (MRF) [34]:

$$MRF = \frac{\bar{\mu}_{90}(n_b)}{n_{MM}}, \tag{5}$$

where n_{MM} is the number of signal events remaining after the cuts, assuming an isotropic magnetic monopole flux with $\phi^0_{MM} = 1.7 \cdot 10^{-13}$ cm$^{-2}\cdot$ s$^{-1}\cdot$ sr^{-1}. In addition to the specific values of the cuts, n_{MM} depends on the detector

acceptance S_{eff} $(cm^2 \cdot sr)$ and on the time period over which data was collected $T(s)$.

In order to compensate for the lack of statistics in the remaining sample of atmospheric muon background, an extrapolation has been perfomed in the region of interest for the signal. An example of extrapolation performed is shown in Fig. 7. After fitting the N_{hit} distribution for muons with an exponential function (red), the latter is extrapolated to the region of interest (pink), then the number of muons remaining after the final cut on N_{hit} is given by the sum of the events from the muon histogram (blue) and the extrapolation (pink).

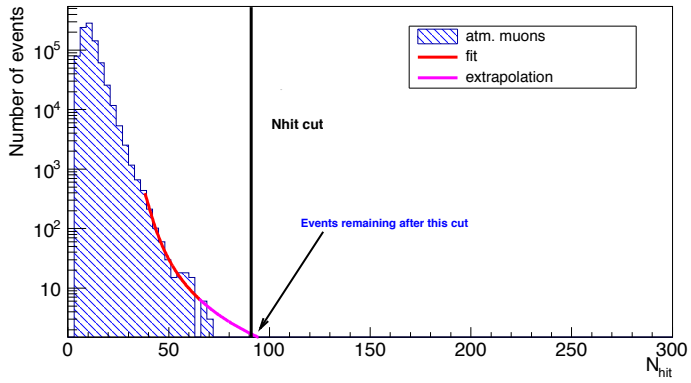

Figure 7: The distribution of N_{hit} for atmospheric muons, extrapolated using an exponential fit function. The contribution of the extrapolation in the total number of events was taken into account in the optimization and the extrapolation uncertainties were computed. For this bin $\beta = [0.8170, 0.8615]$, 1.4 events are found after the cut $N_{hit} \geqslant 91$.

Columns 3 and 4 of Table 1 shows the background expectation, dominated by atmospheric muons, for each bin of β. After the optimization procedure and the estimation of the background, the 90% confidence level upper limit on the magnetic monopole flux is obtained from the values of the cuts yielding the minimum value of the Model Rejection Factor MRF:

$$\phi_{90\%} = \phi^0_{MM} \cdot MRF. \tag{6}$$

The detection efficiency depends on the optical module angular acceptance and the light absorption length in sea water. An evaluation of the

systematic effects due to uncertainties on environmental and detector parameters is presented in [35]. The corresponding systematic uncertainties are negligible compared to the background extrapolation errors quoted in the third column of Table 1, therefore they were ignored in the final limits calculation.

8 Results and discussion

The unblinding was performed on the total set of data collected by the ANTARES telescope during five years, which corresponds to 1012 active days live time after subtracting the 10% burn sample. No significant excess of data events is observed over the expected background, and the upper limits on flux have been found using Eq. (6). Table 1 summarizes, for each of the nine bins of β, the selection cuts, the number of expected background and observed events, and the 90% C.L. upper limits on the magnetic monopole flux.

β range	Selection cuts		Number of	Number of	Number of	Flux Upper Limits at 90%
	α	N_{hit}	atm. muons	atm. neutrinos	observed events	C.L. ($\mathrm{cm^{-2}\cdot\ s^{-1}\cdot\ sr^{-1}}$)
[0.5945, 0.6390]	< 5.5	$\geqslant 36$	1.9 ± 0.8	1.6×10^{-4}	0	5.9×10^{-16}
[0.6390, 0.6835]	< 5.0	$\geqslant 39$	0.9 ± 0.5	1.5×10^{-4}	0	3.6×10^{-17}
[0.6835, 0.7280]	< 3.4	$\geqslant 51$	0.9 ± 1.0	1.2×10^{-4}	0	2.1×10^{-17}
[0.7280, 0.7725]	< 3.3	$\geqslant 51$	1.1 ± 0.5	9.3×10^{-3}	1	9.1×10^{-18}
[0.7725, 0.8170]	< 1.8	$\geqslant 73$	0.6 ± 0.4	1.0×10^{-3}	0	4.5×10^{-18}
[0.8170, 0.8615]	< 0.8	$\geqslant 91$	1.4 ± 0.9	1.8×10^{-1}	1	4.9×10^{-18}
[0.8615, 0.9060]	< 0.6	$\geqslant 92$	1.3 ± 0.8	1.6×10^{-1}		2.5×10^{-18}
[0.9060, 0.9505]	< 0.6	$\geqslant 94$	1.2 ± 0.8	1.3×10^{-1}	0	1.8×10^{-18}
[0.9505, 0.9950]	< 0.6	$\geqslant 95$	1.2 ± 0.7	1.3×10^{-1}	0	1.5×10^{-18}

Table 1: Results after unblinding of the data (1012 active days live time corresponding to 5 years of data taking). The selection cuts, the number of expected (muons and neutrinos) background and observed events and the upper limits on the flux are presented for each range of velocity (β). The table was divided into two parts to distinguish the first five bins where β_{fit} was assumed as a free parameter from the four bins where $\beta_{fit} = 1$.

In the first five bins, the reconstructed velocity β_{fit} was restricted to be compatible with the range of the magnetic monopole velocity. Therefore, the event samples in these ranges are exclusive and must be added. As shown in Table 1, the sum of background events in the first five ranges adds up to 5.4 events whereas only one event has been observed. This indicates a rather conservative method of extrapolating the atmospheric muon sample into the region defined by the final cuts. For the last four bins, $\beta_{fit} = 1$ and cuts on α and N_{hit} are tightened from bin to bin, that means bin 7 is a subset of bin 6 and so on. Thus, the total background is given here by bin 6 already.

In Fig. 8 the ANTARES upper limits as a function of β are presented, together with other experimental results from IceCube [13], MACRO [36] and Baikal [37], as well as the previous result from ANTARES [15] and the theoretical Parker bound [12]. The MACRO experiment was sensitive also to down-going candidates, surviving the ∼3000 meters of water equivalent of the Gran Sasso mountain overburden. Thus, their limit holds for magnetic monopoles of lower mass (starting from 10^6 GeV/c^2). For magnetic monopoles that have to cross the Earth, as in the case of the present paper, the limit is valid for $M > 10^{10}$ GeV/c^2. After applying the final cuts to the unblinded data, two events have been observed. There is one event with $N_{hit} = 93$, $\alpha = 0.5$ and zenith = 27.4° which passes the cuts optimized of two bins of β. It is identified as a bright well-reconstructed neutrino event regarding its physical properties, compatible with the total background observed at this range of high velocities. The second event with $\beta \geq 0.728$ is consistant with a down-going (zenith = 108.1°) atmospheric muon yielding a bright shower.

9 Conclusion

A search for relativistic magnetic monopoles with the ANTARES neutrino telescope has been performed, using data collected during five years (from 2008 to 2012) and corresponding to a total live time of 1012 days. No signal has been observed above the atmospheric background expectation and new upper limits on the monopole flux have been set.

Above the threshold for direct Cherenkov radiation $\beta \geq 0.74$, the limits found are better than those of other neutrino experiments. Below Cherenkov threshold, direct comparison is not straightforward due to the model of cross section used.

Neutrino telescopes are well suited for the search for magnetic monopoles. The future detector KM3NeT [38] will improve the sensitivity to the detection of magnetic monopoles due to its large volume and high detection performance.

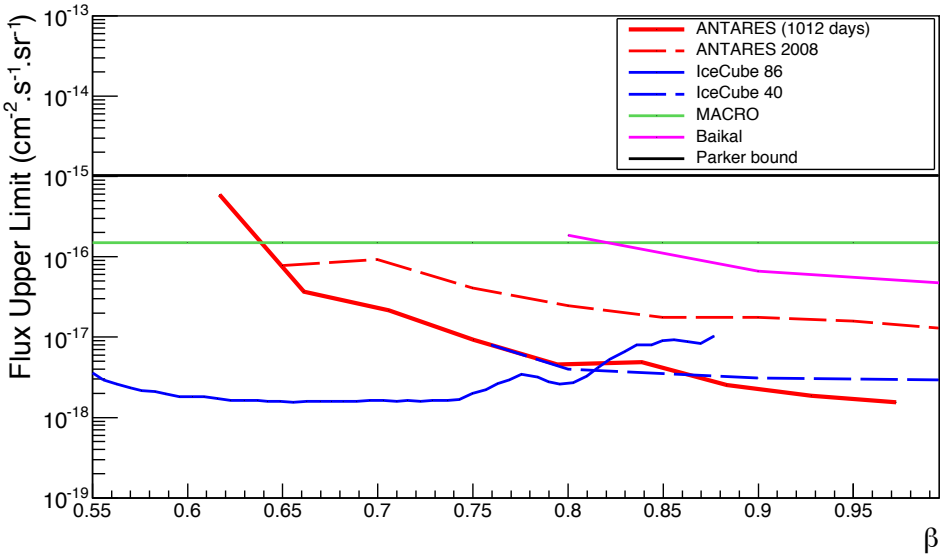

Figure 8: ANTARES 90% C.L. upper limit on flux for magnetic monopoles using five years of data with 1012 active days live time (solid red line), compared to the upper limits obtained by other experiments [13, 36, 37], as well as the previous analysis of ANTARES (dashed red line) [15] and the theoretical Parker bound [12]. In [13] a more optimistic model for δ-rays production of monopoles is used, making a direct comparison difficult.

Acknowledgments

The authors acknowledge the financial support of the funding agencies: Centre National de la Recherche Scientifique (CNRS), Commissariat à l'énergie atomique et aux énergies alternatives (CEA), Commission Européenne (FEDER fund and Marie Curie Program), Institut Universitaire de France (IUF), IdEx program and UnivEarthS Labex program at Sorbonne Paris Cité (ANR-10-LABX-0023 and ANR-11-IDEX-0005-02), Labex OCEVU (ANR-11-LABX-0060) and the A*MIDEX project (ANR-11-IDEX-0001-02), Région

Île-de-France (DIM-ACAV), Région Alsace (contrat CPER), Région Provence-Alpes-Côte d'Azur, Département du Var and Ville de La Seyne-sur-Mer, France; Bundesministerium für Bildung und Forschung (BMBF), Germany; Istituto Nazionale di Fisica Nucleare (INFN), Italy; Stichting voor Fundamenteel Onderzoek der Materie (FOM), Nederlandse organisatie voor Wetenschappelijk Onderzoek (NWO), the Netherlands; Council of the President of the Russian Federation for young scientists and leading scientific schools supporting grants, Russia; National Authority for Scientific Research (ANCS), Romania; Ministerio de Economía y Competitividad (MINECO): Plan Estatal de Investigación (refs. FPA2015-65150-C3-1-P, -2-P and -3-P, (MINECO/FEDER)), Severo Ochoa Centre of Excellence and MultiDark Consolider (MINECO), and Prometeo and Grisolía programs (Generalitat Valenciana), Spain; Ministry of Higher Education, Scientific Research and Professional Training, Morocco. We also acknowledge the technical support of Ifremer, AIM and Foselev Marine for the sea operation and the CC-IN2P3 for the computing facilities.

References

[1] P.A.M. Dirac, *Quantized Singularities in the Electromagnetic Field*, *Proc. R. Soc.* **A 133** (1931) 60.

[2] G. 't Hooft, *Magnetic monopoles in unified gauge theories*, *Nucl. Phys.* **B 79** (1974) 276.

[3] A.M. Polyakov, *Particle Spectrum in the Quantum Field Theory*, *Sov. Phys. JETP Lett.* **20** (1974) 194.

[4] A.H. Guth, *Inflationary universe: A possible solution to the horizon and flatness problems*, *Phys. Rev.* **D 23** (1981) 347.

[5] L. Patrizii and M. Spurio, *Status of Searches for Magnetic Monopoles*, *Ann. Rev. Nucl. Part. Sci.* **65** (2015) 279.

[6] M.W. Ray et al., *Observation of isolated monopoles in a quantum field*, *Science* **348** (2015) 544.

[7] R. Ross et al., *Search for Magnetic Monopoles in Lunar Material Using an Electromagnetic Detector*, *Phys. Rev.* **D 8** (1973) 698.

[8] K. Bendtz et al., *Search for Magnetic Monopoles in Polar Volcanic Rocks*, *Phys. Rev. Lett.* **110** (2013) 121803.

[9] G. Aad et al., *Search for magnetic monopoles and stable particles with high electric charges in 8 TeV pp collisions with the ATLAS detector*, *Phys. Rev.* **D 93** (2016) 052009.

[10] B. Acharya et al., *Search for magnetic monopoles with the MoEDAL prototype trapping detector in 8 TeV proton-proton collisions at the LHC*, *JHEP* **08** (2016) 067.

[11] B. Acharya et al., *Search for magnetic monopoles with the MoEDAL forward trapping detector in 13 TeV proton-proton collisions at the LHC*, *Phys. Rev. Lett.* **118** (2017) 061801.

[12] E.N. Parker, *The Origin of Magnetic Fields*, *Astrophys. J* **160** (1970) 383.

[13] M.G. Aartsen et al., *Searches for Relativistic Magnetic Monopoles in IceCube*, *EPJ* **C76** (2016) 133.

[14] M. Ageron et al., *ANTARES: the first undersea neutrino telescope*, *Nucl. Instr. and Meth.* **A 656** (2011) 11.

[15] S. Adrian-Martinez et al., *Search for Relativistic Magnetic Monopoles with the ANTARES Neutrino Telescope*, *Astropart. Phys.* **35** (2012) 634.

[16] J.A. Aguilar et al., *The data acquisition system for the ANTARES neutrino telescope*, *Nucl. Instr. and Meth.* **A 570** (2007) 107.

[17] D.R. Tompkins, *Total energy loss and Cerenkov emission from monopoles*, *Phys. Rev.* **138** (1965) 248.

[18] Y. Kazama et al., *Scattering of a Dirac particle with charge Ze by a fixed magnetic monopole*, *Phys. Rev.* **D 15** (1977) 2287.

[19] S.P. Ahlen, *Monopole-track characteristics in plastic detectors*, *Phys. Rev.* **D 14** (1976) 2935.

[20] S.P. Ahlen, *Stopping-power formula for magnetic monopoles*, *Phys. Rev.* **D 17**, 1 (1978) 229.

[21] J. Derkaoui et al., *Energy losses of magnetic monopoles and of dyons in the earth*, *Astropart. Phys.* **9** (1998) 173.

[22] D. Ryu et al., *Cosmic magnetic fields in large scale filaments and sheets*, *Astron. Astrophys.* **335** (1998) 19.

[23] *Application Software Group, GEANT, CERN Program Library Long Writeup W5013* (1993), http://wwwasd.web.cern.ch/wwwasd/geant/.

[24] G. Carminati et al., *Atmospheric MUons from PArametric formulas: a fast GEnerator for neutrino telescopes (MUPAGE)*, *Comput. Phys. Commun.* **179(12)** (2008) 915.

[25] Y. Becherini et al., *A Parameterisation of single and multiple muons in the deep water or ice*, *Astrop. Phys.* **25** (2006) 1.

[26] J. Brunner, *ANTARES simulation tools, Proceedings of the VLVnT 2003, Amsterdam (http://www.vlvnt.nl/proceedings.pdf).*

[27] A. Margiotta, *Common simulation tools for large volume neutrino detectors*, *NIM* **A725** (2013) 98.

[28] V. Agrawal et al., *Atmospheric neutrino flux above 1 GeV*, *Phys. Rev.* **D 53** (1996) 1314.

[29] G.D. Barr et al., *Uncertainties in atmospheric neutrino fluxes*, *Phys. Rev.* **D 74** (2006) 094009.

[30] L. Fusco and A. Margiotta, *The Run-by-Run Monte Carlo simulation for the ANTARES experiment*, *EPJ Web of Conferences* **116** (2016) 02002.

[31] J.A. Aguilar et al., *A fast algorithm for muon track reconstruction and its application to the ANTARES neutrino telescope*, *Astropart. Phys.* **34** (2011) 652.

[32] S. Adrian-Martinez et al., *Searches for Point-like and extended neutrino sources close to the Galactic Centre using the ANTARES neutrino Telescope*, *Astrophys. J. Lett.* **786:L5** (2014) arxiv:1402.6182.

[33] G.J. Feldman and R.D. Cousins, *Unified approach to the classical statistical analysis of small signals*, *Phys. Rev.* **D 57** (1998) 3873.

[34] G.C. Hill and K. Rawlins, *Unbiased cut selection for optimal upper limits in neutrino detectors: themodel rejection potential technique*, *Astropart. Phys.* **19** (2003) 393.

[35] J.A. Aguilar et al., *Zenith distribution and flux of atmospheric muons measured with the 5-line ANTARES detector*, *Astropart. Phys.* **34** (2010) 179.

[36] M. Ambrosio et al., *Final results of magnetic monopole searches with the MACRO experiment*, *Eur. Phys. J.* **C 25** (2002) 511.

[37] V. Aynutdinov et al., *Search for relativistic magnetic monopoles with the Baikal neutrino telescope*, *Astropart. Phys.* **29** (2008) 366.

[38] S. Adrian-Martinez et al., *Letter of intent for KM3NeT 2.0.*, *J. Phys.* **G43(8)** (2016) 084001.